Sensors and Materials, Vol. 28, No. 3 (2016) 231–236
MYU Tokyo

S & M 1173

Effects of Sintering Temperature on the Response of $CuFeTe_2$ Ceramics to Oxygen Gas

Masatoshi Kozaki,* Yuta Tokunaga, Yezhi Huang, Hisao Kuriyaki, and Kiyoshi Toko

Graduate School of Information Electrical Engineering, Kyushu University,
744 Motooka, Nishi-ku, Fukuoka 819-0395, Japan

(Received September 18, 2015; accepted December 25, 2015)

Keywords: oxygen gas sensor, intercalation, layered material

A new oxygen sensor based on the resistance change caused by oxygen intercalation in the layered compound $CuFeTe_2$ (CFT) was developed. When intercalation occurs, oxygen molecules penetrate into the CFT interlayer, stretching the van der Waals gap and increasing the *c*-axis resistance. In this study, we prepared ceramic samples from a single crystal using different sintering temperatures. Results show that the sample sintered at 100 °C showed the highest oxygen gas response. Moreover we carried out the surface observation of the cross section of each CFT ceramic sample and found that the porosity of the sample increased with decreasing sintering temperature.

1. Introduction

Nowadays, oxygen sensors are important devices in daily life. The most popular type of oxygen sensor is the zirconia (zirconium dioxide) oxygen sensor. This type of oxygen sensor requires a high temperature (about 400 °C) to operate. Hence, its power consumption is high. To reduce power consumption, a room temperature oxygen sensor has been developed. The only sensor of this type is the galvanic cell oxygen sensor. Therefore, we are developing a new type of room-temperature oxygen sensor with a new mechanism using the intercalation phenomenon.[1,2]

The layered compound $CuFeTe_2$ (CFT) is a semiconductor with a layered structure (tetragonal; lattice parameters: $a = 0.394$ nm and $c = 0.678$ nm). In the crystalline structure of CFT, unit layers consisting of three atomic planes, i.e., Te, *M* (= Cu or Fe), and Te in that order, are stacked in the *c*-direction while sandwiching van der Waals (vdW) gaps.[3,4] Because of these gaps, a strong cleavage in the direction perpendicular to the c-plane is generated.

The reversible insertion of a molecule or ion into the vdW gap of compounds with layered structures is known as intercalation, and the removal of a molecule or ion is known as deintercalation. Lithium-ion batteries of cell phones are typical applications of intercalation/deintercalation.[5] In other studies, other applications of intercalation/deintercalation, such as an odor sensor and a photo-rechargeable battery using intercalation, have also been reported.[6–8]

New types of oxygen sensors that can operate at room temperature using the intercalation of oxygen molecules for the layered compounds TiS_2 and CFT have been developed.[9,10] We have found that the resistance in the *c*-direction of these compounds reversibly changes with the partial

*Corresponding author: e-mail: m.kouzaki@nbelab.ed.kyushu-u.ac.jp

ISSN 0914-4935

oxygen pressure under a total pressure of 1 atm. This phenomenon is considered to be due to the lengthening in the *c*-direction owing to the expansion of the vdW gaps between CFT layers because of the intercalation of oxygen molecules. In our previous work, single-crystal CFT thin films micro fabricated by wet etching using photolithography were developed for use as a layered compound CFT.[10] The response time of the single-crystal CFT thin film to oxygen gas decreased with the formation of many fine pores through microfabrication.

In this study, we prepared ceramic samples from a $CuFeTe_2$ single crystal using different sintering temperatures. Moreover, we examined the difference in response to oxygen gas between CFT ceramic samples sintered at several temperatures, and we observed the cross section of the surface of each CFT ceramic sample.

2. Materials and Methods

2.1 Preparation of CFT ceramics

Single-crystal CFT was grown by the vertical Bridgman method, as described in our previous study.[10] The ingot was pulverized and sieved with a 20-μm-pore-size sieve. After that, the powder was uniaxially pressed (2 tons/cm^2) into a pellet with a thickness of about 0.2 mm. The pellet was cut into a rectangle (2 × 7 mm^2) and then sintered at 100–450 °C for 10 h under a vacuum of less than 10^{-4} Pa.

2.2 Measurement method

The oxygen gas sensing properties of CFT were measured in a flow-type apparatus, as shown in Fig. 1. Changes in the resistance of the CFT ceramic samples in the *c*-direction were measured by the four-point probe method using 50-μm-diameter copper wire and silver paste. The oxygen concentration was precisely controlled using a flow system with a mass flow controller. The total flow was 200 mL/min. After pure nitrogen gas was allowed to flow, gas mixtures of oxygen + nitrogen were allowed to flow for 30 min, and then the flow gas entering the chamber was changed to pure nitrogen.

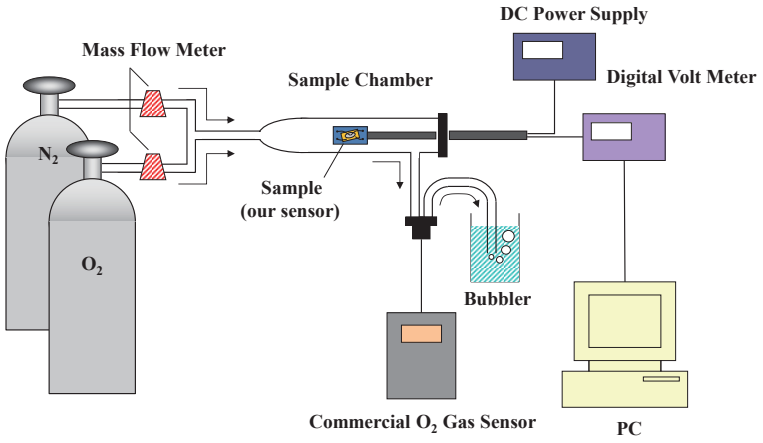

Fig. 1. (Color online) Mass flow and measurement system.

2.3 Preparation of CFT for scanning electron microscopy (SEM) analysis

To prepare each ceramic sample for observation, the ceramic sample was buried using resin and its cross section was ground. Subsequently, a 5-μm platinum coating was formed on the cross section using an auto fine coater (JEOL JFC-1600), and the cross section was observed by SEM.

3. Results and Discussion

Figure 2 shows the normalized resistance of the CFT ceramic samples sintered at different temperatures in response to oxygen gas. The response signal was defined as the normalized resistance, which was the ratio of the electrical resistances of the samples in an oxygen gas with N_2 carrier gas and in only N_2 carrier gas.

When 50% oxygen gas was introduced into the sample chamber, oxygen molecules intercalated to increase the resistance, which then saturated at a certain value. A reproducible response to oxygen gas was obtained when oxygen and nitrogen gases were alternately introduced into the sample chamber. When nitrogen gas was introduced after the introduction of oxygen gas, the resistance decreased to its initial value owing to the deintercalation of oxygen molecules. The values of normalized resistances of the CFT ceramic samples sintered at 100 and 550 °C were 1.9 and 0.5%, respectively, suggesting that the use of ceramics with a low sintering temperature results in high sensitivity. Figures 3 and 4, respectively, show the dependence of electrical resistance on oxygen concentration for the CFT ceramics sintered at 100 and 550 °C. The normalized resistance also increased with the oxygen gas concentration. Figure 5 shows the relationship between $\Delta R/R$ and the oxygen gas concentration. $\Delta R/R$ was defined as the average value of the three measured values before 100% N_2 carrier gas was introduced into sample chamber. Error bars show the standard deviation of $\Delta R/R$. The sample sintered at 100 °C showed higher $\Delta R/R$ values than that sintered at 550 °C at all oxygen concentrations. We also prepared a non-sintered sample. The non-sintered sample could not be measured because of its fragility.

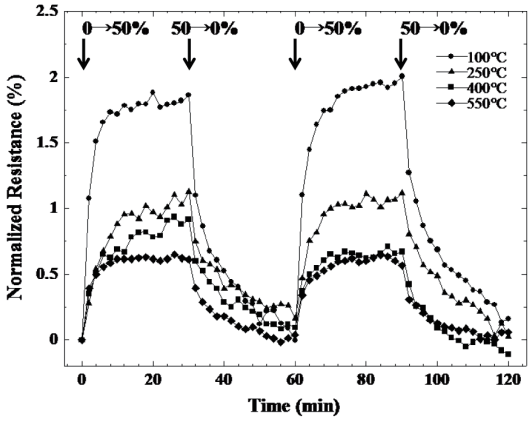

Fig. 2. Response to 50% oxygen concentration of the samples prepared at different sintering temperatures.

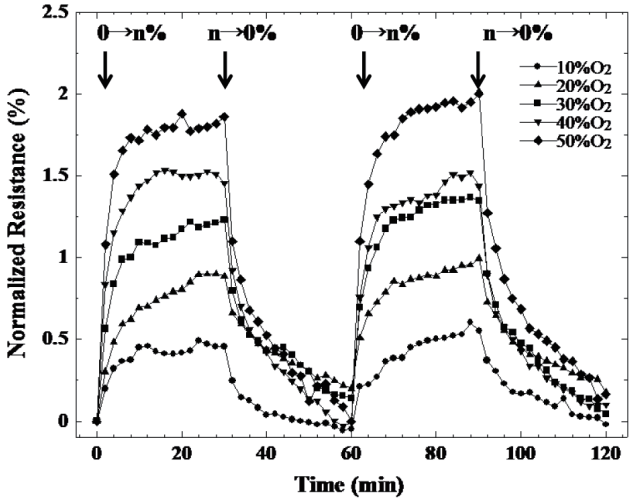

Fig. 3. Response to oxygen concentration of the CFT sample sintered at 100 °C.

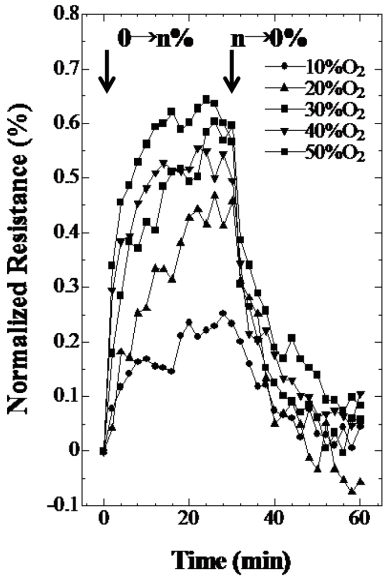

Fig. 4. Response to oxygen concentration of the CFT sample sintered at 550 °C.

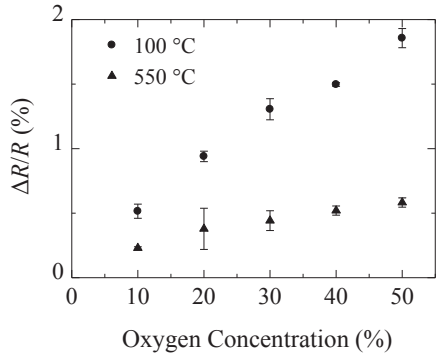

Fig. 5. Saturation values of the normalized resistances of the two samples sintered at 100 and 550 °C.

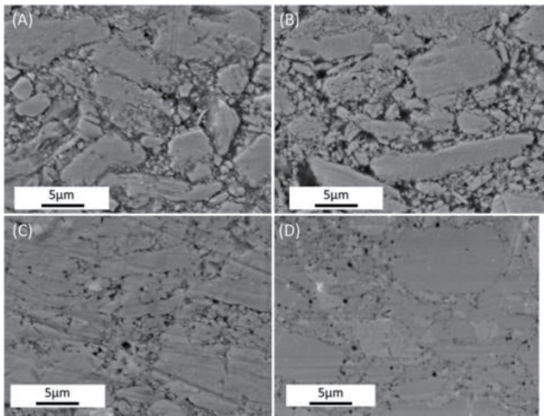

Fig. 6. Cross-sectional SEM images of the samples prepared at different sintering temperatures: (A) 100, (B) 250, (C) 400, and (D) 550 °C.

Figure 6 shows cross-sectional SEM images of the CFT ceramic samples sintered at different temperatures. The SEM images show porous structures and 5–20 μm-sized-grains. The SEM images for the microstructural characterization of the ceramics were analyzed by the image digital processing software Image J.[11,12] The porosity was determined by SEM with Image J. As shown in Fig. 7, the porosity was calculated from the difference in the brightness of the SEM image in the grain area and porous areas. When the sintering temperatures were 100, 250, 400, and 550 °C, the porosities were 30.9, 25.2, 19.6, and 18.0%, respectively. The porosity decreased with increasing

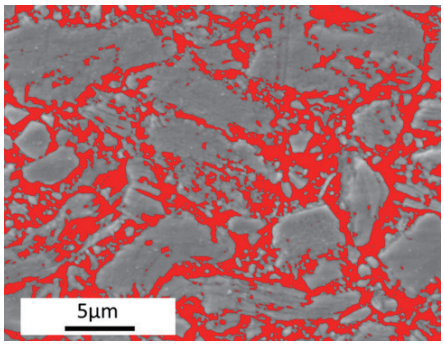

Fig. 7. (Color online) Semi automatic porosity segmentation, carried out using Image J, by automatic thresholding (sintering temperature of samples was 100 °C).

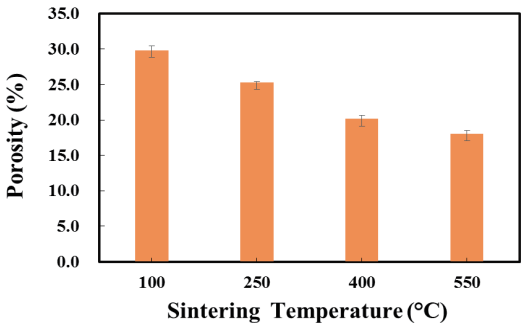

Fig. 8. (Color online) Relationship between sintering temperature and porosity.

sintering temperature (Fig. 8). This means that as the sintering temperature increases, the sintering process develops, the crystal grains grow, and the porous area decreases. From the oxygen gas responses and SEM results, the space in CFT ceramics that can intercalate oxygen molecules as well as the $\Delta R/R$ value were found to decrease with the increase in sintering temperature.

4. Conclusions

CFT ceramic samples with different sintering temperatures ware developed. A reproducible response of the CFT samples to oxygen gas was confirmed by measuring the resistance of the samples when nitrogen and oxygen gases were alternately introduced. The changes in the resistances of the CFT ceramic samples sintered at 100 and 550 °C were 1.9 and 0.5%, respectively. According to the results of SEM, the space in CFT ceramics that can intercalate oxygen molecule of CFT decreased because of the increase in sintering temperature. Thus, it was demonstrated that reducing the sintering temperature of CFT ceramics is effective for increasing the sensor response. We plan to change the grain size of the CFT ceramics and consider the most suitable fabrication conditions because commercially available oxygen sensors exhibit a response time of 0.5 min or less. We expect further improvement of the oxygen sensor parameters.

Acknowledgements

The image of the cross section of each CFT ceramic sample was obtained by SEM at the Center of Advanced Instrumental Analysis, Kyushu University.

References

1 H. Kuriyaki, K. Kishiro, and K. Hirakawa: Jpn. J. Appl. Phys. **29** (1990) 1604.
2 K. Kishiro, H. Kuriyaki, and K. Hirakawa: Jpn. J. Appl. Phys. **32** (1993) 674.
3 F. N. Abdullaev, T. G. Kerimova, G. D. Sultanov, and N. A. Abdullaev: Phys. Solid State **48** (2006) 1848.
4 A.Rivas-Mendoza, F. González-Jiménez, J. M. Broto, H. Rakoto, and J. González: Rev. Cubana de Fisica. **28** (2011) 14.

5 M. Yoshio and H. Noguchi: Lithium-Ion Batteries, ed. M.Yosio, R. J. Brodd, and A. Kozawa (Springer, New York, 2008) Chap 2.
6 T. Itoh, I. Matsubara, W. Shin, N. Izu, and M. Nishibori: J Ceram. Soc. Jpn. **118** (2010) 171.
7 T. Nomiyama, H. Kuriyaki, and K. Hirakawa: Synth. Met. **71** (1995) 2237.
8 Z. X. Shu, R. S. McMillan, and J. J. Murray: J. Electrochem. Soc. **140** (1993) 922.
9 K. Kishiro, S. Takemoto, H. Kuriyaki, and K. Hirakawa: Jpn. J. Appl. Phys. **33** (1994) 1069.
10 M. Kozaki, Y. Higuchi, A. Ikeda, H. Kuriyaki, and K. Toko: Sensor. Mater. **25** (2013) 471.
11 C. A. Schneider, W. S. Rasband, and K. W. Eliceiri: Nat. Methods **9** (2012) 671.
12 S. Hemes, G. Desbois, J. L. Urai, B. Schröppel, and J. Schwarz: Microporus Mesoporus Mater. **208** (2015) 1.